CrossMark

RESEARCH PAPER

Agglomeration behavior of lipid-capped gold nanoparticles

Rajeev Ranjan · Maria A. Kirillova ·
Elena N. Esimbekova · Sergey M. Zharkov ·
Valentina A. Kratasyuk

Abstract The current investigation deciphers aggregation pattern of gold nanoparticles (AuNPs) and lipid-treated AuNPs when subjected to aqueous sodium chloride solution with increasing ionic strengths (100–400 nM). AuNPs were synthesized using 0.29 mM chloroauric acid and by varying the concentrations of trisodium citrate (AuNP1 1.55 mM, AuNP2 3.1 mM) and silver nitrate (AuNP3 5.3 μM, AuNP4 10.6 μM) with characteristic LSPR peaks in the range of 525–533 nm. TEM analysis revealed AuNPs to be predominantly faceted nanocrystals with the average size of AuNP1 to be 35 ± 5 nm, AuNP2 15 ± 5 nm, AuNP3 30 ± 5 nm, and AuNP4 30 ± 5 nm and the zeta-average for AuNPs were calculated to be 31.23, 63.80, 26.08, and 28 nm respectively. Induced aggregation was observed within 10 s in all synthesized AuNPs while lipid-treated AuNP2 (AuNP2-L) was found to withstand ionic interferences at all concentration levels. However, lipid-treated AuNPs synthesized using silver nitrate and 1.55 mM trisodium citrate (AuNP3, AuNP4) showed much lower stability. The zeta potential values of lipid-treated AuNPs (AuNP1-L-1x/200, -17.93 ± 1.02 mV; AuNP2-L-1x/200, -21.63 ± 0.70; AuNP3-L-1x/200, -14.54 ± 0.90; AuNP3-L-1x/200 -13.77 ± 0.83) justified these observations. To summarize, AuNP1 and AuNP2 treated with lipid mixture 1 equals or above 1x/200 or 1x/1000 respectively showed strong resistance against ionic interferences (up to 400 mM NaCl). Use of lipid mixture 1 for obtaining highly stable AuNPs also provided functional arms of various lengths which can be used for covalent coupling.

R. Ranjan · M. A. Kirillova · E. N. Esimbekova (✉) ·
V. A. Kratasyuk
Laboratory of Bioluminescent Biotechnologies, Department of Biophysics, Institute of Fundamental Biology and Biotechnology, Siberian Federal University, 79 Svobodny prospect, Krasnoyarsk, Russia 660041
e-mail: esimbekova@yandex.ru

E. N. Esimbekova · V. A. Kratasyuk
Institute of Biophysics, Federal Research Center 'Krasnoyarsk Science Center SB RAS', Akademgorodok 50/50, Krasnoyarsk, Russia 660036

S. M. Zharkov
Kirensky Institute of Physics, Federal Research Center 'Krasnoyarsk Science Center SB RAS', Akademgorodok 50/38, Krasnoyarsk, Russia 660036

S. M. Zharkov
Electron Microscopy Laboratory, Siberian Federal University, 79 Svobodny prospect, Krasnoyarsk, Russia 660041

Introduction

Functionalized nanomaterials and hybrid nanostructures have greatly contributed to technological advancements in wide areas of research such as bio-remediation (Showkat et al. 2007), solar energy harvest

(Narkeviciute et al. 2016), photo-luminescence enhancement (Hassan et al. 2014), waste water purification (Reddy et al. 2014), electromagnetic nanocomposites (Reddy et al. 2008a), and nano-electronic/opto-electronic devices (Reddy et al. 2007; Reddy et al. 2008b).

Role of gold nanoparticles (AuNPs) in designing versatile and tunable biosensing formats is huge (Ranjan et al. 2017a, b; Abhijith et al. 2014; Thakur et al. 2013). AuNPs possess enhanced opto-electronic properties and much higher extinction coefficient. Further, AuNPs show comparatively lower toxicity so as to be exploited for in vivo sensing and designing therapeutic strategies as well (Khlebtsov and Dykman 2011; Fratoddi et al. 2015). Numerous colorimetric biosensing design is based on the principle of AuNP aggregation which can be seen in determination and quantification of numerous analytes of high importance such as biothiols (Ghasemi et al. 2015), cancer cells (Borghei et al. 2016), organophosphorous pesticides (Kim et al. 2015), potassium ions, S-adenosyl homocysteine hydrolase activity, and heavy metals such as mercury and lead (Lin et al. 2010; Gao et al. 2015; Thatai et al. 2016).

Investigation of salt-induced aggregation kinetics of AuNPs would be very useful in realizing the optimal performance of novel biosensing strategies. In cue of this, it is believed that salt-induced AuNP aggregation is supposedly due to hampering of uniformly distributed negative charge around them (Sun et al. 2016). Further, mechanistic description of AuNP synthesis would be very helpful in understanding their relative stability when obtained via different routes. In general, AuNP synthesis is observed in overall three subsequent steps viz. nucleation, aggregation, and capping (Engelbrekt et al. 2013; Wuithschick et al. 2015). One of the most commonly investigated AuNPs are citrate capped. Easy synthetic routes and versatile applications have owed to their popularity. Citrate capping effectively creates an anionic shielding around the reduced Au core (Au^0), thereby maintaining their individual integrity. However, they tend to agglomerate under the influence of metal ions especially Na^+ and Mg^{2+}. In this regard, interaction of Mg^{2+} ions with gallic acid-coated AuNPs was studied. Selective quenching of UV-Vis absorbance even at 200 ppb was observed (Kim et al. 2017). In vitro applications of AuNPs are huge and are mostly colorimetric based (Priyadarshini and Pradhan 2017; Li et al. 2017). However, in vivo investigations using AuNPs require robustness in terms of enhanced resistance against ionic interference. Synthesis of ultra-stable and biocompatible

AuNPs is highly desired in the area of real-time bioimaging, drug delivery, photodynamic therapy, plasmonics, and biosensors (Kalakonda and Sreenivas 2017; Hamilton et al. 2017; Aioub and El-Sayed 2016). Gupta et al. (2016) have also indicated the disadvantages of unstable AuNPs and have advocated the use of non-ionic poly(ethylene glycol) and zwitterionic ligand (carboxybetaine) for stabilizing AuNPs. Reports on lipid-capped AuNPs have also been seen recently in the work of Kang and Ko (2015) where they used lipids such as DPPC, DPPG, cholesterol, DOTAP, and PEG2K-DSPE to obtain cationic and anionic lipid-coated AuNPs. However, the procedure was quite tedious which involved harmful organic solvents, overnight drying, long duration mixing, and ultrasonication. Further, Dichello et al. (2017) developed methods to entrap cationic and anionic nanoparticles within liposomes following a three step strategy. Use of organic solvents and their subsequent removal by evaporation was seen as a cumbersome process.

Therefore, in the current investigation, our aim was to stabilize AuNPs following a simple, convenient, and ecofriendly approach. In this regard, a sparingly soluble lipid mixture 1 was used as an agent to stabilize citrate-capped AuNPs. Moreover, the study aimed to optimize the lipid ratio as a stabilizing agent to synthesized AuNPs via much simpler routes. To the best of our knowledge, the present investigation is a novel approach to obtain ultra-stable AuNPs without the involvement of harmful organic solvents and tedious experimental procedures.

Materials and methods

Materials

Hydrogen tetrachloroaurate (III) trihydrate ($HAuCl_4 \cdot 3H_2O$) was procured from Alfa Aesar (ThermoFisher Inc., Karlsruhe, Germany) while trisodium citrate was purchased from PanReac AppliChem GmbH, Germany. Silver nitrate ($AgNO_3$) was from LLC Ural Chemicals Plant, Moscow, Russia. Chemically defined lipid mixture 1 was the product of Sigma-Aldrich, St. Louis, MO, USA. Sodium chloride (NaCl) was the product of Medigen, Novosibirsk, Russia. Nitric acid (HNO_3) and hydrochloric acid (HCl) were purchased from Giredmet, Moscow, Russia. Glycerol and magnetic beads were purchased locally. All the

reagents used in this study were of analytical grade and extra pure.

Methods

Synthesis of AuNPs

All the glasswares (three-neck round bottom flask, glass stoppers, beakers, pipettes, reflux condenser) used in the experiments were thoroughly washed and put in aqua regia solution (mixture of HCl and HNO_3 in the ratio 3:1) to eliminate any traces of impurities followed by rinsing with double distilled water. The glasswares were put in hot air oven for drying until further use. Stock solution of $HAuCl_4 \cdot 3H_2O$ (0.1 M) was prepared by dissolving 0.393 g of $HAuCl_4 \cdot 3H_2O$ in ultrapure water to obtain 10 mL aqueous solution and kept at 4 °C under dark while 0.1% of $AgNO_3$ aqueous stock solution was prepared by dissolving 2 mg of $AgNO_3$ in 2 mL of ultrapure water and used immediately.

AuNPs were prepared using the method described previously (Abhijith et al. 2014) with minor modifications. Four different types of AuNPs were prepared where AuNP1 and AuNP2 contained 20 and 40 mg of trisodium citrate (2 mL) respectively and 145 μL of $HAuCl_4 \cdot 3H_2O$ (0.1 M) while AuNP3 and AuNP4 had 45 and 90 μL of 0.1% $AgNO_3$ respectively with 20 mg trisodium citrate and 145 μL of $HAuCl_4 \cdot 3H_2O$ (0.1 M) in common.

In brief, 145 μL of $HAuCl_4 \cdot 3H_2O$ (0.1 M) was added to 5 mL of water followed by addition of freshly prepared aqueous solution of trisodium citrate (2 mL) and different aliquots of silver nitrate stock solution (0.1%). The final volume was adjusted up to 10 mL and kept for 10 min incubation after gentle mixing under dark.

Meanwhile, reflux set up was arranged in which 40 mL of ultrapure water was put in the round bottom flask and kept for boiling under condensation using glycerol as the heat transfer medium kept in a glass jar. The heating was performed using a magnetic stirrer with heating facility (RH basic 2, IKA, Germany). A magnetic bead was inserted in the round bottom flask, and the boiling water was allowed to stir. The aqueous mixture of chloroauric acid, trisodium citrate, and/or silver nitrate was added to the round bottom flask, and the solution was allowed to react for a period of 15 min. The obtained color solution was cooled and kept in glass vials for further study. The final concentration of each reactants were as follows: for AuNP1: $HAuCl_4 \cdot 3H_2O$ 0.29 mM, trisodium citrate 1.54 mM; for AuNP2: $HAuCl_4 \cdot 3H_2O$ 0.29 mM, trisodium citrate 3.08 mM; for AuNP3: $HAuCl_4 \cdot 3H_2O$ 0.29 mM, trisodium citrate 1.54 mM, silver nitrate 5.3 μM; and for AuNP4: $HAuCl_4 \cdot 3H_2O$ 0.29 mM, trisodium citrate 1.54 mM, silver nitrate 10.6 μM.

Synthesis of lipid-capped AuNPs

Formation of lipid-capped AuNPs (AuNP-L) was carried out by the addition of lipid mixture 1 to the AuNPs in different proportions ($1x/1000$, $1x/500$, $3x/1000$, $1x/200$, and $1x/50$, total volume 5 mL, where x represents lipid mixture 1) followed by pulsed sonication using an ultrasonicator probe MS 73 (Sonopuls HD 3100, Bandelin electronic GmbH & Co. KG, Germany) for 1 s (four times) with successive 2 s interval, 0.048 KJ at the amplitude of 80%. Aggregation studies for AuNP-L were carried out following the same procedures as described previously.

Sodium chloride-induced aggregation assay

Sodium chloride-induced AuNP aggregation was carried out at three different molar strengths (100, 200, and 400 mM) for which a 5-M stock solution of NaCl was prepared using ultrapure water and added to the synthesized AuNPs to a final volume of 1 mL. The absorbance spectra for the AuNPs were recorded using UV-Vis spectrophotometer (Cary 60, Agilent technologies, USA) before and after the addition of NaCl at the time intervals of 10 and 30 s and 1 and 2 min.

Size, shape, and chemical characterization

Transmission electron microscopy (TEM) analysis was carried out placing a droplet of individual AuNPs on ultrathin carbon type A and formvar on 400 mesh Cu grid (Ted Pella, USA) followed by passive drying at room temperature. JEM-2100 transmission electron microscope equipped with an energy dispersive spectrometer (EDS) Oxford Inca x-sight (JEOL, Tokyo, Japan) operating at 200 kV was used for TEM imaging, phase, and elemental analysis.

Zeta potential and size measurements were carried out using Zetasizer Nano ZS (Malvern Instruments Ltd., UK). Synthesized AuNPs were pipetted individually in disposable folded capillary cells for zeta potential measurement at 25 °C. Size measurements were performed

using 3 mL disposable cuvettes with the scattering angle of 173°.

Results and discussion

Absorption and peak characteristics of AuNPs and AuNPs-L

The absorption spectra for the synthesized AuNPs and AuNPs-L are shown in Fig. 1. The absorption maxima were found to be in the range of 533–525 nm for the synthesized AuNPs. The yield of AuNP1 was the least while AuNP2 absorbed the light spectrum maximally. Absorbance peak of 525 nm was the characteristic of AuNP3 (Fig. 1 (a)). Lipid-capped AuNPs were also analyzed for their absorption spectrum as shown in Fig. 1 (b). The graph indicates red-shift of 1–2 nm in AuNPs with slight increase in their absorbance. The highest red-shift was observed in case of AuNP1-L-1x/200 while highest increase in absorbance was seen in case of AuNP4-L-1x/200. Increased absorbance in lipid-

treated AuNPs can be attributed to lowering of transmittance caused due to the formation of lipid layer around the individual AuNPs. Shift of peak wavelength ensures close interaction of lipid with the AuNPs with increase in their size (Remant Bahadur et al. 2006).

TEM, ED, and EDS analysis

TEM analysis (Fig. 1 (a', b', c, and d)) revealed that the synthesized AuNPs were mainly faceted nanocrystals. The size of AuNP1 was in the range of 25–50 nm with the average diameter of 35 ± 5 nm. AuNP2, AuNP3, and AuNP4 had the particle size in the range of 10–25 nm, 17–40 nm, and 10–45 nm respectively while predominantly, the average size was measured to be 15 ± 5 nm for AuNP2, AuNP3 (30 ± 5 nm), and AuNP4 (30 ± 5 nm). The energy dispersive spectroscopy (EDS) showed that AuNP3 and AuNP4 had an average weight % of Ag as 1.5 ± 0.5 and 2.5 ± 0.5 respectively. It is worth mentioning that the EDS spectra obtained from the individual AuNP corresponded to higher Ag concentration with the decreasing particle size (Fig. S1 and
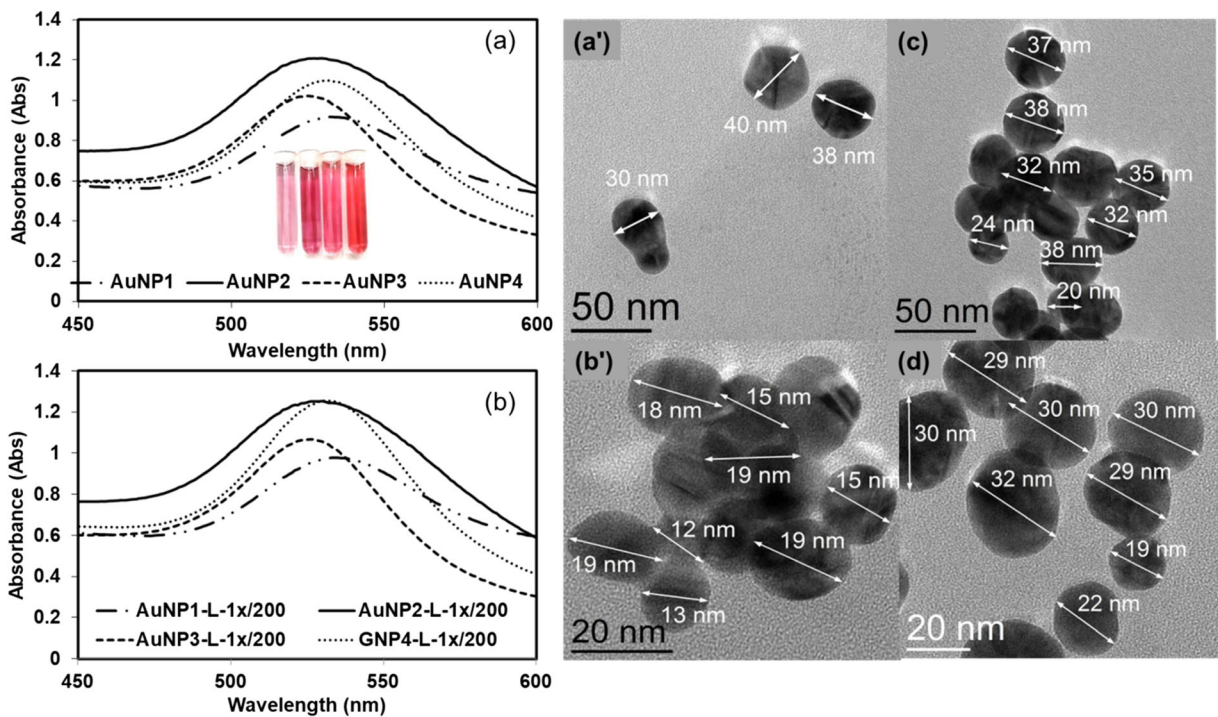

Fig. 1 (a) Absorption spectra of AuNP1 (λ_{max} 532 nm, Abs 0.92); AuNP2 (λ_{max} 529 nm, Abs 1.2); AuNP3 (λ_{max} 525 nm, Abs 1.02), and AuNP4 (λ_{max} 531 nm, Abs 1.01) and (b) absorption spectra of AuNP1-L-1x/200 (λ_{max} 534 nm, Abs 0.98), (b) AuNP2-L-1x/200

(λ_{max} 530 nm, Abs 1.25), AuNP3-L-1x/200 (λ_{max} 526 nm, Abs 1.07), and AuNP4-L-1x/200 (λ_{max} 531 nm, Abs 1.25). Transmission electron microscopy images for (a') AuNP1, (b') AuNP2, (c) AuNP3, and (d) AuNP4

ST1). It can be explained by the idea that in the case when Au nanoparticles of different size are covered with a layer of Ag of a fixed thickness, the proportion of Ag to Au will increase with the decreasing Au nanoparticle size. The electron diffraction (ED) pattern obtained from AuNP3 is shown in Fig. S2. The ED pattern is typical for all the synthesized AuNPs. The interpretation of the electron diffraction reflections (ST2) indicates that all the observed reflections correspond to the face central cubic phase of Au (space group Fm-3m, lattice constant $a = 4.0786$ Å). It should be noted that Au and Ag have the same type of crystal structure and the difference in their lattice constants is less than 0.2%. This is the reason why the ED patterns obtained from AuNP1 and AuNP2 containing pure Au and those obtained from AuNP3 and AuNP4 containing Au and Ag do not differ.

Zeta potential and size measurement

The obtained results for the zeta potential and size measurements are presented in Table 1. Zeta potential for AuNP2 was found to be -49.47 ± 0.81 mV (maximum value) while -36.43 ± 1.27 (minimum value) for AuNP4. The negative values for the zeta potential were attributed to the negatively charged citrate capping around the Au^0 core. There is a clear indication of partial shielding of negative charge in citrate-capped AuNP3 and AuNP4 by Ag^+ ions. EDS measurements strongly support this observation of decrease in zeta potential with increase in % wt. of Ag^+.

The result justifies the stability pattern of AuNPs in the order indicated as AuNP2 > AuNP1 > AuNP3 >

AuNP4 in their native form. However, post lipid mixture 1 treatment, the zeta potential was found to marginally decrease in all the AuNPs-L which is the indicative of successful lipid capping in agreement with previous reports (Dichello et al. 2017). The zeta-average of the AuNPs were in the order AuNP2 > AuNP1 > AuNP4 > AuNP3 while post lipid treatment, the zeta-average of AuNP3-L-1x/200 increased by 1.7 times than AuNP3, thereby changing the trend as AuNP2 > AuNP3 > AuNP1 > AuNP4. The intensity of peak area 1 was found to be in the range of 80–100% while intensity of peak area 2 lied in the range of 8–20%. The third peak area intensity was insignificant (0–2.9%) which was seen only in case of AuNP1-L-1x/200, AuNP3-L-1x/200, and AuNP4-L-1x/200.

Interestingly, when zeta-average data were compared with TEM measurements, all the synthesized AuNPs correlated well except AuNP2 (Fig. 1 (b') and Table 1). The TEM image showed the average size of AuNP2 to be 15 ± 5 nm while zeta-average was estimated to be 63.80 nm which was marginally high. This observation suggests the impeccable role of trisodium citrate in efficient capping around the Au^0 core in AuNP2 which had led to increase the hydrodynamic diameter.

Agglomeration pattern of AuNPs and AuNPs-L

Sodium chloride-led rapid agglomeration was observed in all AuNPs undertaken in this study. Citrate-capped AuNPs surrounds the gold core (Au^0), and inter-ionic repulsive forces prevent AuNPs to coalesce and

Table 1 TEM diameter, zeta-average size, potential, and their distribution in synthesized AuNPs before and after the treatment with lipid mixture 1

Sample name	TEM, diameter (nm)	Zeta-average, diameter (nm)	Polydispersity (PDI)	Peak 1 mean intensity diameter (nm)	Peak 2 mean intensity diameter (nm)	Peak 3 mean intensity diameter (nm)	Peak 1 area intensity (%)	Peak 2 area intensity (%)	Peak 3 area intensity (%)	Zeta potential (mV)
AuNP1	35 ± 5	31.23	0.51	61.13	5.87	0	86.7	13.3	0	− 37.8 ± 0.66
AuNP2	15 ± 5	63.80	0.54	145.47	25.47	0	80.25	19.75	0	− 49.47 ± 0.81
AuNP3	30 ± 5	26.08	0.51	53.83	7	0	82.77	17.23	0	− 36.83 ± 0.15
AuNP4	30 ± 5	28	0.463	54.61	5.30	0	88.7	11.3	0	− 36.43 ± 1.27
AuNP1-L-1x/200		39.88	0.553	79.96	6.617	3974	85.6	11.6	2.9	− 17.93 ± 1.02
AuNP2-L-1x/200		78.45	0.561	169.3	0	0	100	0	0	− 21.63 ± 0.70
AuNP3-L-1x/200		44.96	0.503	84.25	11.73	4587	80.7	16.2	3.1	− 14.54 ± 0.90
AuNP4-L-1x/200		35.86	0.419	58.98	7.18	4077	89.5	8.7	1.9	− 13.77 ± 0.83

aggregate eventually (Piella et al. 2016). However, ionic interferences drastically hamper this anionic shielding by binding to the citrate ions and causing neutralization. As a result, AuNPs settle down and lose their plasmonic properties. During this phase, their characteristic plasmonic peak broadens and shows decreased absorption (Kim et al. 2008). Figure 2a–c depicts such phenomena when AuNP1 was subjected to NaCl solution. Within 10 s, the absorbance peak of AuNP1 was seen to decrease by ca. 40% and continued this trend further, reaching to 90%. Broadening of peak and shift of plasmonic peak towards red region (up to 6 nm) was observed leading to purple-blue appearance of AuNPs. Peak broadening indicates non-uniform aggregation of AuNPs leading to formation of particles of varied size (Han et al. 2011). Figure 2d shows the control values during the study which indicated negligible decrease in absorbance even at 8% aqueous dilution required during analysis of samples at 400 mM strength of NaCl.

In contrast to our previous findings using AuNP1-C (Fig. 2), lipid-treated AuNPs (AuNP1-L-1x/200) withstood against NaCl solution at all concentration levels (Fig. 3). No broadening of peaks or appreciable absorption decrease was observed implying their enhanced

stability. Lipid mixture 1 consists of sparingly soluble non animal-derived fatty acids such as arachidonic, linoleic, linolenic, myristic, oleic, palmitic, and stearic acid apart from cholesterol, tween-80, tocopherol acetate, and Pluronic F-68. It was presumed that AuNPs treated with lipid mixture 1 forms a hydrophobic layer surrounding the citrate-capped region while exposing carboxylic acid (–COOH) predominantly as hydrophilic exterior with varied arm lengths. This observation was further supported with the zeta potential and size measurements for the AuNPs before and after treatment with lipid mixture 1 (Table 1). In spite of more than 50% decrease in zeta potential, AuNP1-L and AuNP2-L showed enhanced stability against NaCl led-induced aggregation. Therefore, it becomes evident that zeta potential is not the only criterion in deciding the stability of colloidal solutions. Nevertheless, AuNP-L-1x/200 showed the magnitude of zeta potential to be ca. 7 units higher than AuNP3-L and AuNP4-L which is in agreement to the dependence of colloidal stability on the values of zeta potential.

In our opinion, this hydrophobic coating prevented sodium ions to access citrate ions and ultimately neutralize them. Additionally, these multifunctional arms
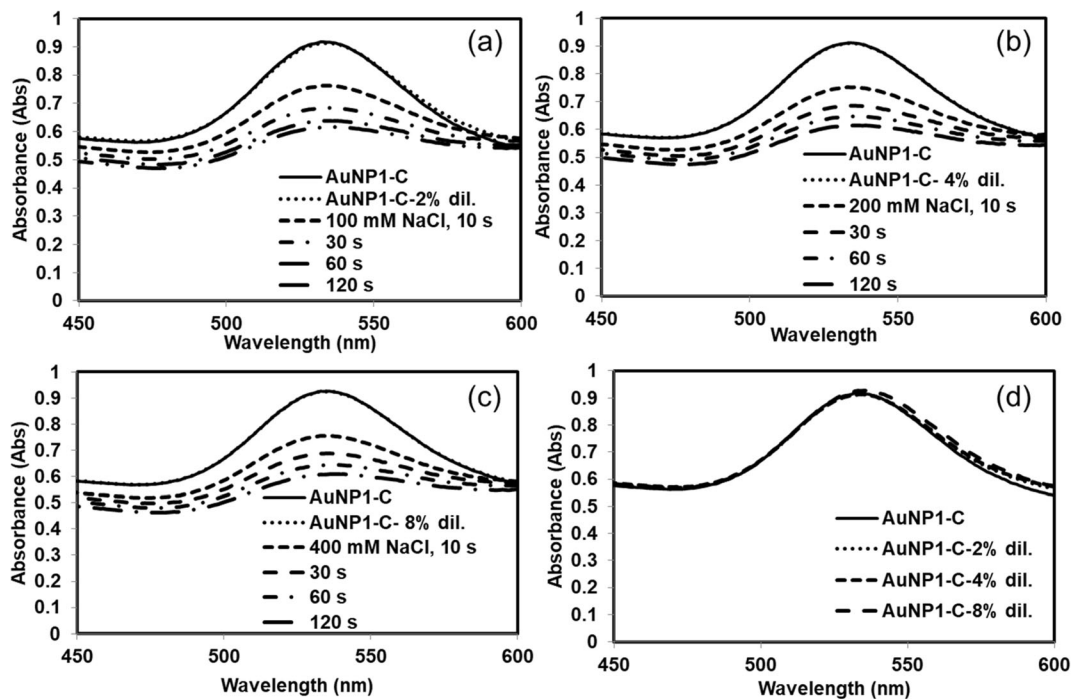

Fig. 2 The aggregation pattern of AuNP1, where AuNP1-C shows the control value while (AuNP1-C- 2% dil.) indicates 2% aqueous dilution and likewise. **a**, **b**, and **c** The effect of aqueous NaCl solution on the absorption spectra of AuNP1 at 100, 200, and 400 mM respectively. **d** The effect of aqueous dilutions on the absorbance spectra which served as control values
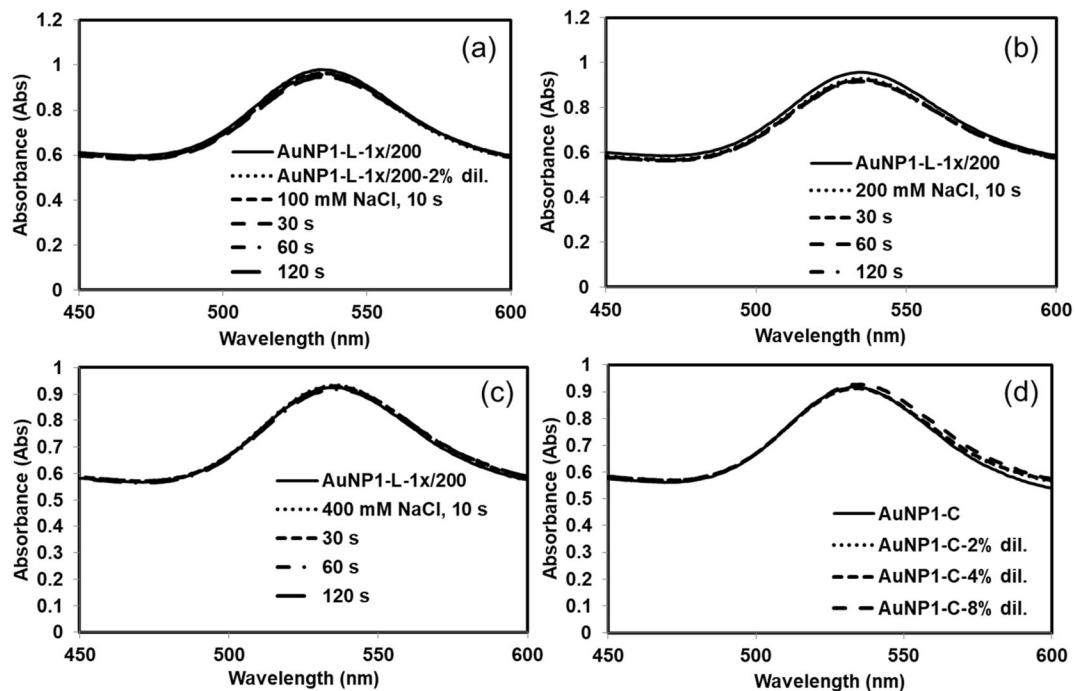
Fig. 3 The absorbance spectra were found to be fairly superimposed in **a**, **b**, and **c** at 100, 200, and 400 mM of sodium chloride solution respectively. AuNP1-L-1*x*/200 indicates lipid-treated AuNP1 in the ratio of 1:200 where *x* represents Lipid mixture 1. **d** Served as control absorbance values. No peak shift was observed in all cases

with hydrophilic exterior might have prevented sufficient neutralization by monosodium ions (Na$^+$) so as to initiate agglomeration. The other possibility for this extraordinarily high stability may be due to hydrophobicity of the individual AuNPs preventing AuNPs to coalesce. The optimal concentration of stabilizing agent (lipid mixture 1) was found to be 1*x*/200 in the case of AuNP1-L. Studies showed that at 1*x*/1000 and 1*x*/500 lipid content, aggregation of AuNP1-L was observed at all concentration levels of the aggregation agent, i.e., NaCl (Fig. 4a–f).

In this case, although the aggregation process was slower in comparison to aggregation pattern of AuNP1 (Fig. 2), we observed color change towards bluish-purple in AuNP-L-1*x*/500 over time. At 3*x*/1000 concentration levels, aggregation of AuNP1-L was not observed at 100 mM NaCl but at higher strengths (200 and 400 mM NaCl), gradual decrease in absorbance was seen implying delayed aggregation (Fig. 4g–i).

Therefore, AuNP1-L-1*x*/200 was found to be the most suitable to withstand against ionic interferences. We further investigated the role of citrate ions in stabilization of AuNPs by synthesizing AuNP2 which used

trisodium citrate twice the previous concentration that was used for the synthesis of AuNP1. Doubling the concentration of trisodium citrate led to the formation of AuNP2 with higher yield (Abs: 1.2) with respect to AuNP1 (Abs: 0.92) (Fig. 1 (a)).

The aggregation pattern of AuNP2-L was observed to differ significantly in comparison to AuNP1. In this case, the peak shift and its subsequent broadening was seen towards the red region and was more pronounced (Fig. 5a–c) while stability of AuNP2-L-1*x*/200 was intact (Fig. 5d–f). Further, stability of AuNP2-L was studied at lower concentrations of lipid mixture 1 (1*x*/1000, 1*x*/500, and 3*x*/1000) as shown in Fig. 6. The result showed striking difference in AuNP2-L stability in comparison to AuNP1-L. Even at the least concentration of lipid mixture 1 (1*x*/1000) that was used in obtaining AuNP2-L-1*x*/1000, negligible decrease in absorbance was seen unlike in the case of AuNP1-L (1*x*/1000–3*x*/1000) (Fig. 6a–c) and (Fig. 4a–c) respectively.

The result emphasized the role of trisodium citrate in enhanced stability when treated with lipid mixture 1.
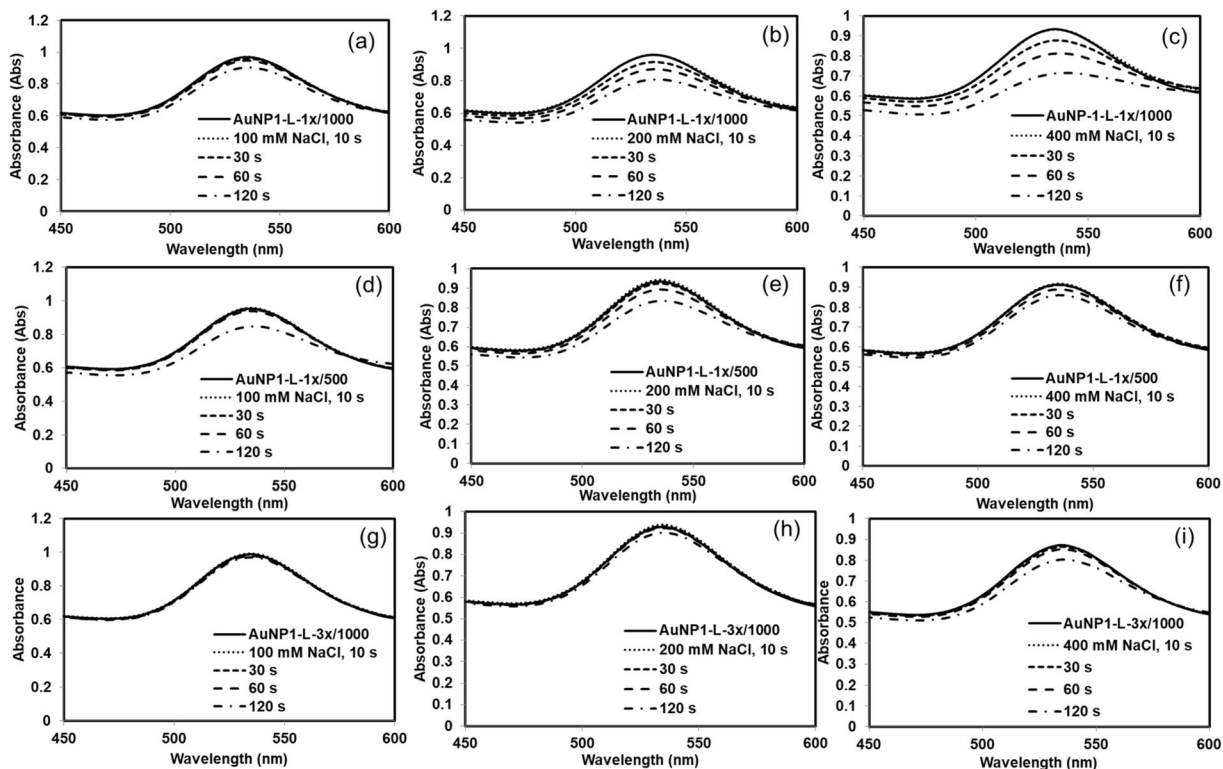
Fig. 4 a–i The effect of Lipid mixture 1 on the stability of AuNP1 at concentration levels of 1x/1000, 1x/500, and 3x/1000 is presented in the presence of aqueous NaCl solution at 100 mM, 200 mM, and 400 mM. Negligible absorbance decay was observed in g indicating optimal level lipid (3x/1000) which could withstand up to 100 mM NaCl. In contrast, c suggests highest agglomeration rate of AuNP1-L-1x/1000

The possible explanation for this observation may lie in improved shielding of AuNP2-L from ionic interferences.

However, when we carried out our further investigation on AuNPs synthesized using AgNO₃ as additional component (AuNP3 and AuNP4), we saw an entirely
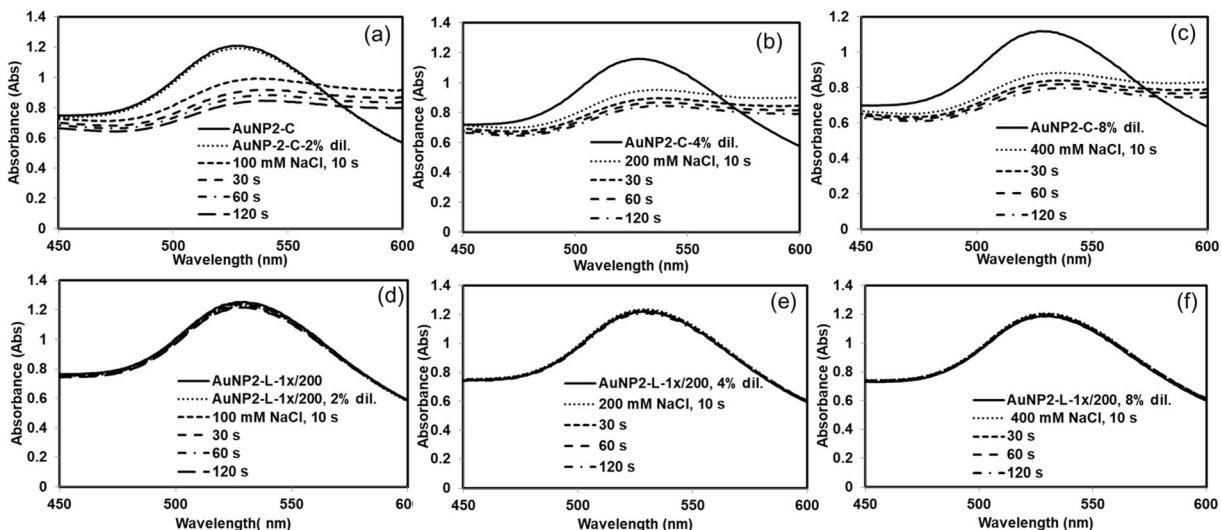

Fig. 5 a–c The ca. 40% absorbance decay with concomitant broadening of peak shifting towards the red region. In contrast, d–f show the superimposition of absorption spectra indicating strong resistance of AuNP2-L-1x/200 against NaCl at 100–400 mM
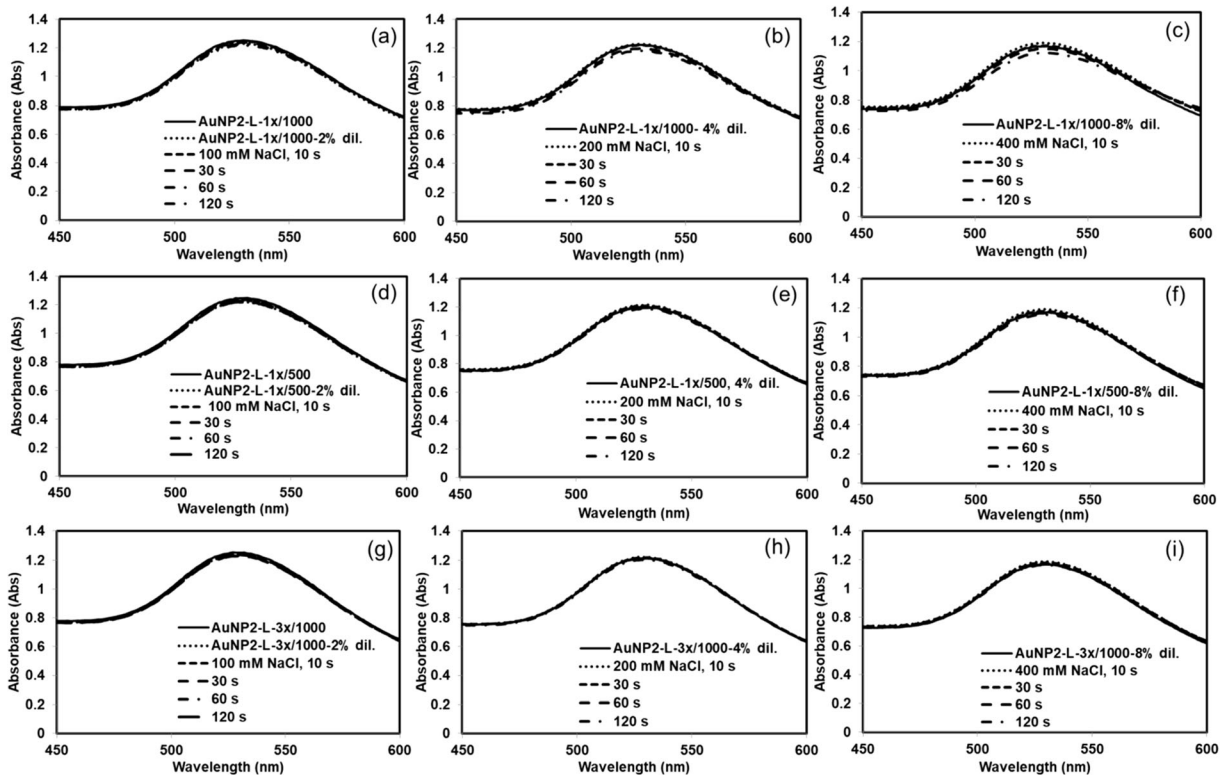
Fig. 6 **a**, **d**–**i** AuNP-2-L at all levels show no absorbance decay, and the absorption spectra shows superimposed most prominently except **b** and **c**

different scenario. The stability of AuNP3-L and AuNP4-L was dramatically reduced. NaCl-led aggregation was found to be strikingly higher in AuNP3-L-1*x*/200 as shown in Fig. 7.

Although the rate of decrease of absorbance was slightly lower than AuNP3-C (Fig. S3), however, more than 90% aggregation was witnessed within a period of 2 min.

The result was baffling since we did not expect that Ag$^+$ ions with as low as 5.3 μM can bring such huge difference in AuNP stability. Further, AuNP3-L-1*x*/50 was investigated where quantity of stabilizing agent used was fourfold to see the stabilization effect at 100 mM NaCl (Fig. S4) but the trend of absorption decay remained almost the same.

In order to confirm the role of Ag$^+$ ions in destabilization of AuNPs, AuNP4 was synthesized by doubling the AgNO$_3$ concentration in the reaction mixture. In this case, we started our aggregation study at 100 mM NaCl and found neither AuNP4 nor AuNP4-L-1*x*/200 had any stability against ionic interference which confirmed the striking effect of

Ag$^+$ ions in destabilization of lipid capping in AuNP4 (Fig. S5). However, the rate of absorbance decrease in AuNP4-L-1*x*/200 was slightly less than in the case of AuNP4. We further lowered down the strength of NaCl up to 20 mM to learn the absorbance pattern of AuNP4 and AuNP4-L (Fig. S5 c, d). In this case, we observed decay rate of AuNP4-L to be much lower than their counterpart suggesting rudimentary role of lipid mixture 1 as stabilizing agent. At 40 mM, a similar observation was marked (Fig. S5 e, f). In spite of these results, it became evident that Ag$^+$ ion played a significant negative role in lipid-based stabilization of AuNPs. Ag$^+$ of AgNO$_3$ is a shape guiding, catalytic agent which has higher surface enhancement factor in comparison to Au (Abhijith et al. 2014).

The zeta-size measurements confirm lipid capping in AuNP3-L and AuNP4-L; however, the magnitude of zeta potential was found to decrease than their counterparts. EDS analysis strongly supported the role of Ag$^+$ ions in shielding the AuNP3 and AuNP4 by forming a layer. It is likely
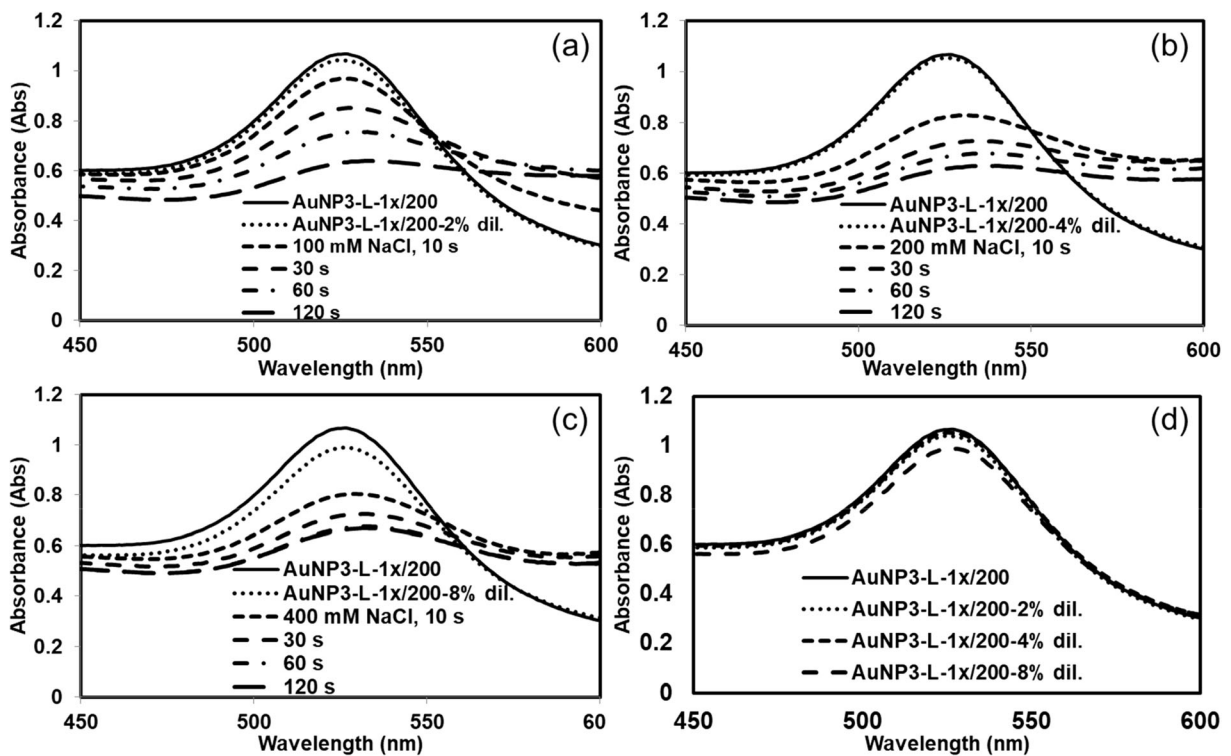
Fig. 7 **a–c** Aggregation pattern of AuNP3 in presence of 100–400 mM NaCl. **d** Served as control values at different aqueous dilutions

that this layer of Ag around AuNP3 and AuNP4 is involved in supporting destabilization of these AuNPs against ionic interferences.

Conclusion

Stability issues of AuNPs delimit their scope of application especially towards in vivo research. Use of lipid-stabilized AuNPs for such research directions have been emerged as an auspicious tool. The present approach through the utilization of lipid mixture 1 as stabilizing agent was found to be very useful in obtaining ultra-robust AuNPs with multidimensional and multifunctional capabilities. Arm lengths of different lengths carrying –COOH functional moiety allow easy functionalization using coupling chemistry. The possible applications of AuNPs-L is tremendously huge especially in bioimaging, metal-enhanced bioluminescence studies, photodynamic therapies, drug delivery, and in the design of AuNP-based point-of-care devices. The AuNPs-L has a very high shelf life and resists agglomeration even at 400 mM sodium

chloride strength. Easy synthesis without the requirement of hazardous organic solvents is some of the key features of these AuNPs.

Compliance with ethical standards

Conflict of interest   The authors declare that they have no conflict of interest.

References

Abhijith KS, Sharma R, Ranjan R, Thakur MS (2014) Facile synthesis of gold–silver alloy nanoparticles for application in metal enhanced bioluminescence. Photochemical & Photobiological Sciences 13(7):986–991

Aioub M, El-Sayed MA (2016) A real-time surface enhanced Raman spectroscopy study of plasmonic photothermal cell death using targeted gold nanoparticles. J Am Chem Soc 138(4):1258–1264

Borghei YS, Hosseini M, Dadmehr M, Hosseinkhani S, Ganjali MR, Sheikhnejad R (2016) Visual detection of cancer cells by colorimetric aptasensor based on aggregation of gold nanoparticles induced by DNA hybridization. Anal Chim Acta 904:92–97

Dichello GA, Fukuda T, Maekawa T, Whitby RL, Mikhalovsky SV, Alavijeh M, Pannala AS, Sarker DK (2017) Preparation of liposomes containing small gold nanoparticles using electrostatic interactions. Eur J Pharm Sci 105:55–63

Engelbrekt C, Jensen PS, Sørensen KH, Ulstrup J, Zhang J (2013) Complexity of gold nanoparticle formation disclosed by dynamics study. J Phys Chem C 117(22):11818–11828

Fratoddi I, Venditti I, Cametti C, Russo MV (2015) How toxic are gold nanoparticles? The state-of-the-art. Nano Res 8(6):1771–1799

Gao ZF, Song WW, Luo HQ, Li NB (2015) Detection of mercury ions (II) based on non-cross-linking aggregation of double-stranded DNA modified gold nanoparticles by resonance Rayleigh scattering method. Biosens Bioelectron 65:360–365

Ghasemi F, Hormozi-Nezhad MR, Mahmoudi M (2015) A colorimetric sensor array for detection and discrimination of biothiols based on aggregation of gold nanoparticles. Anal Chim Acta 882:58–67

Gupta A, Moyano DF, Parnsubsakul A, Papadopoulos A, Wang LS, Landis RF, Das R, Rotello VM (2016) Ultrastable and biofunctionalizable gold nanoparticles. ACS Appl Mater Interfaces 8(22):14096–14101

Hamilton DJ, Coffman MD, Knight JD, Reed SM (2017) Lipid-coated gold nanoparticles and FRET allow sensitive monitoring of liposome clustering mediated by the synaptotagmin-7 C2A domain. Langmuir 33(36):9222–9230

Han X, Goebl J, Lu Z, Yin Y (2011) Role of salt in the spontaneous assembly of charged gold nanoparticles in ethanol. Langmuir 27(9):5282–5289

Hassan M, Haque E, Reddy KR, Minett AI, Chen J, Gomes VG (2014) Edge-enriched graphene quantum dots for enhanced photoluminescence and supercapacitance. Nano 6(20):11988–11994

Kalakonda P, Sreenivas B (2017) Synthesis and optical properties of highly stabilized peptide-coated gold nanoparticles. Plasmonics 12(4):1221–1225

Kang JH, Ko YT (2015) Lipid-coated gold nanocomposites for enhanced cancer therapy. Int J Nanomed 10(Spec Iss):33–45

Khlebtsov N, Dykman L (2011) Biodistribution and toxicity of engineered gold nanoparticles: a review of in vitro and in vivo studies. Chem Soc Rev 40(3):1647–1671

Kim T, Lee CH, Joo SW, Lee K (2008) Kinetics of gold nanoparticle aggregation: experiments and modeling. J Colloid Interface Sci 318(2):238–243

Kim MS, Kim GW, Park TJ (2015) A facile and sensitive detection of organophosphorus chemicals by rapid aggregation of gold nanoparticles using organic compounds. Biosens Bioelectron 67:408–412

Kim DY, Shinde S, Ghodake G (2017) Tuning stable and unstable aggregates of gallic acid capped gold nanoparticles using Mg 2+ as coordinating agent. J Colloid Interface Sci 494:1–7

Li B, Li X, Dong Y, Wang B, Li D, Shi Y, Wu Y (2017) Colorimetric sensor array based on gold nanoparticles with diverse surface charges for microorganisms identification. Anal Chem 89(20):10639–10643

Lin JH, Chang CW, Wu ZH, Tseng WL (2010) Colorimetric assay for S-adenosylhomocysteine hydrolase activity and inhibition using fluorosurfactant-capped gold nanoparticles. Anal Chem 82(21):8775–8779

Narkeviciute I, Chakthranont P, Mackus AJ, Hahn C, Pinaud BA, Bent SF, Jaramillo TF (2016) Tandem core–shell Si–Ta_3N_5 photoanodes for photoelectrochemical water splitting. Nano Lett 16(12):7565–7572

Piella J, Bastús NG, Puntes V (2016) Size-controlled synthesis of sub-10-nanometer citrate-stabilized gold nanoparticles and related optical properties. Chem Mater 28(4):1066–1075

Priyadarshini E, Pradhan N (2017) Gold nanoparticles as efficient sensors in colorimetric detection of toxic metal ions: a review. Sensors Actuators B Chem 238:888–902

Ranjan R, Esimbekova EN, Kirillova MA, Kratasyuk VA (2017a) Metal-enhanced luminescence: current trend and future perspectives—a review. Anal Chim Acta 971:1–13

Ranjan R, Esimbekova EN, Kratasyuk VA (2017b) Rapid biosensing tools for cancer biomarkers. Biosens Bioelectron 87:918–930

Reddy KR, Lee KP, Gopalan AI (2007) Self-assembly directed synthesis of poly (ortho-toluidine)-metal (gold and palladium) composite nanospheres. J Nanosci Nanotechnol 7(9):3117–3125

Reddy KR, Lee KP, Gopalan AI (2008a) Self-assembly approach for the synthesis of electro-magnetic functionalized Fe 3 O 4/polyaniline nanocomposites: effect of dopant on the properties. Colloids Surf A Physicochem Eng Asp 320(1):49–56

Reddy KR, Sin BC, Yoo CH, Park W, Ryu KS, Lee JS, Sohn D, Lee Y (2008b) A new one-step synthesis method for coating multi-walled carbon nanotubes with cuprous oxide nanoparticles. Scr Mater 58(11):1010–1013

Reddy KR, Gomes VG, Hassan M (2014) Carbon functionalized TiO_2 nanofibers for high efficiency photocatalysis. Materials Research Express 1(1):015012

Remant Bahadur KC, Aryal S, Bhattarai SR, Bhattarai N, Kim CH, Kim HY (2006) Stabilization of gold nanoparticles by hydrophobically-modified polycations. J Biomater Sci Polym Edit 17(5):579–589

Showkat AM, Zhang YP, Kim MS, Gopalan AI, Reddy KR, Lee K (2007) Analysis of heavy metal toxic ions by adsorption onto amino-functionalized ordered mesoporous silica. Bull Kor Chem Soc 28(11):1985–1992

Sun M, Liu F, Zhu Y, Wang W, Hu J, Liu J, Dai Z, Wang K, Wei Y, Bai J, Gao W (2016) Salt-induced aggregation of gold nanoparticles for photoacoustic imaging and photothermal therapy of cancer. Nano 8(8):4452–4457

Thakur MS, Ranjan R, Vinayaka AC, Abhijith KS, Sharma R (2013) Nanoparticles and biophotonics as efficient tools in resonance energy transfer-based biosensing for monitoring food toxins and pesticides. In: Park B, Appell M (eds) Advances in applied nanotechnology for agriculture. American Chemical Society, Washington, D.C., pp 55–84

Thatai S, Khurana P, Prasad S, Soni SK, Kumar D (2016) Trace colorimetric detection of Pb^{2+} using plasmonic gold nanoparticles and silica–gold nanocomposites. Microchem J 124:104–110

Wuithschick M, Birnbaum A, Witte S, Sztucki M, Vainio U, Pinna N, Rademann K, Emmerling F, Kraehnert R, Polte J (2015) Turkevich in new robes: key questions answered for the most common gold nanoparticle synthesis. ACS Nano 9(7):7052–7071